Desalination and Water Treatment
www.deswater.com

doi: 10.1080/19443994.2015.1128364

57 (2016) 22000–22016
October

Taylor & Francis
Taylor & Francis Group

Removal of tetrabromobisphenol-A from aqueous solution by Al_{13}-Montmorillonite modified with different types of surfactants and transition metals

Xiang Li[a,b], Qian Deng[a,b], Zaili Zhang[a,b], Xiaoshan Jia[a,b,*]

[a]*School of Environmental Science and Engineering, Sun Yat-Sen University, Guangzhou 510275, China, Tel. +86 20 39332690; emails: lix53@mail2.sysu.edu.cn (X. Li), 1141486962@qq.com (Q. Deng), eeszzl@mail.sysu.edu.cn (Z. Zhang), eesjxs@126.com (X. Jia)*

[b]*Guangdong Provincial Key Laboratories of Environmental Pollution Control and Remediation Technology, Sun Yat-Sen University, Guangzhou 510275, China*

Received 25 March 2015; Accepted 22 November 2015

ABSTRACT

In this study, remediation of tetrabromobisphenol-A (TBBPA) from aqueous solution by sorption using transition metals-modified inorganic–organic montmorillonite (IOMt) was demonstrated. The adsorbents were prepared in two steps: (1) intercalation of surfactants into Al_{13}-pillared montmorillonite for synthesizing two types of IOMt; (2) incorporation of transition metals (Cu^{2+}, Ni^{2+}, or Co^{2+}) onto those IOMts. Firstly, these materials were characterized by XRD, FTIR, TGA, SEM-EDS, and BET analyses. Then, experiments were conducted on the sorption isotherms, kinetics, and thermodynamics of TBBPA. In general, sorption process with Cu- and Ni-modified IOMt achieved higher TBBPA removal efficiency than sorption process with original IOMt. The modified IOMt displayed the sorption capacity that varied depending on TBBPA initial concentration, pH, and metals loading. However, the type of surfactants did not influence TBBPA sorption on metals-modified IOMt. This probably indicated that complex interaction between TBBPA and metals rather than hydrophobicity plays a key factor in TBBPA sorption process. Equilibrium data could be well interpreted by the Freundlich model, and the rate of sorption was adjusted to a pseudo-second-order kinetic model. The negative values of Gibbs energy change (ΔG) and positive values of enthalpy change (ΔH) indicated the spontaneous and endothermic nature of process.

Keywords: Transition metals; Montmorillonite; TBBPA; Sorption; Inorganic–organic

1. Introduction

Sorption plays an important role in removing hazardous materials from liquid phases; therefore, it has attracted considerable attention in scientific research in the past three decades. Activated carbon is the most well-known used adsorbent. The porous nature of this adsorbent material and its high internal surface area are favorable for sorption. However, high

*Corresponding author.

cost and recovering problem of activated carbon particles from treated water are its disadvantage [1]. In recent years, inorganic–organic clays (IOCYs) complexes have been considered as alternative low-cost adsorbents because of their variety of application and excellent properties [2–6]. The permanent negative charge within the crystal structure of clay materials make them suitable for surface modification by long-chain or short-chain organic surfactants. Through ion exchange, hydrophilic clays can be converted to hydrophobic organic clays that showed a high affinity to hydrophobic organic contaminants (HOCs). The pillared clay with inorganic polyoxocation not only possesses unique microporous structural characteristics, excellent thermal stability, and a large BET surface area as an ideal catalyst supporting materials, but also possesses a higher effective charge. Furthermore, by introducing inorganic polyoxocation and surfactant molecule into the interlamellar space, those materials simultaneously remove HOCs and oxy-anionic contaminants from water, which make them excellent adsorbents of contaminants from aqueous solution [7–12].

The transition metals could form stable complexes with many compounds containing N-donor group, O-donor group, and aromatic groups. Since the processes are dominated by weak chemical interaction, formation of such complexes onto the surface of an adsorbent could provide the basis for the removal of aromatics while still permitting regeneration via accessible engineering. Recent studies indicated that transition metals could enhance the sorption of contaminants on IOCYs when the transition metals were incorporated into the IOCYs [10–12]. They also suggested that the incorporation of transition metals into IOCYs could become a potential strategy for the bottom-up design of adsorbents tailored for the highly selective removal of aromatic pollutants [10,11].

Tetrabromobisphenol-A (TBBPA) is one of the aromatic pollutants and has been widely detected in the environmental samples from around the world, including Japan, Sweden, and the US [13–15]. Due to the extensive use of TBBPA, bioconcentration potential in aquatic organisms, and observed toxicity, it is important to eliminate TBBPA from aqueous water [16]. Although researchers have intensively studied sorption mechanism of TBBPA onto different adsorbents, for example, graphene oxide [16], soil [17] and multiwalled carbon nanotubes [18], sorption of TBBPA on modified clays is still scant. In addition, since TBBPA had benzene rings and O-donor groups, it was probable that transition metals could form stable complexes with TBBPA and enhance TBBPA uptake by inorganic–organic montmorillonite (IOMt). Thus, sorption of TBBPA from aqueous solution onto original IOMt and transition metals-modified IOMt were performed in this study. The main aim of this study was to evaluate sorption mechanism and determine effects of transition metals on sorption process. Furthermore, IOMt are prepared by incorporating cationic surfactant trimethyl ammonium bromide (TMAB) or mixture of anionic surfactant sodium stearate (SSTA) and TMAB to Al_{13}-pillared montmorillonite. Transition metals including copper(II), cobalt(II), and nickel(II) are utilized to synthesize transition metals-modified IOMt. Sorption isotherms, kinetics, and thermodynamics of TBBPA are also investigated in bath experiments. This work could provide a potential strategy for the development of modified clays for TBBPA removal.

2. Materials and methods

2.1. Materials

The TBBPA (97% purity, Mw 543.9 g/mol, CAS number 79-94-7) was purchased from Sigma Chemical Co., Ltd (USA). The selected physicochemical properties of TBBPA are given in Table 1. The K10 montmorillonite (Mt) was obtained from Aladdin Chemistry Co., Ltd (Shanghai, China). The cation-exchange capacities (CECs) of montmorillonite were 44.3 meq/100 g. Cation surfactant-cetyltrimethylammonium bromide (TMAB) and anion surfactant sodium stearate (SSTA) were obtained from Bio Science &Technology. Co., Ltd (Shanghai, China). Methanol is of HPLC grade and purchased from Fisher Co., Ltd (Shanghai, China). The ultrapure water was obtained directly from a Nanopure UV deionization system, Barnstead/Thermolyne Co., Ltd (Dubuque, IA, USA). All other chemicals were of analytical grade unless the stated otherwise.

2.2. Preparation of IOMt modified by transition metals

Aluminum (Al_{13})-pillared montmorillonite (AMt) was prepared using an aluminum chloride solution and following methods reported elsewhere [19]. TMAB intercalated AMt were prepared by dispersing the AMt in solution of TMAB (0.04 M) for 6 h in water bath at 60˚C. The amount of AMt used during the dispersions was 20 g. Afterward, the suspension was filtered by vacuum filtration and washed several times with distilled water until the Br- was not detected by Ag_2SO_4 solution. The obtained clays were dried at 65˚C, activated for 1 h at 105˚C. For reference, the materials that resulted from intercalation will be known as TAMt. SSTA-modified TAMt were prepared by dispersing the TAMt in solution of SSTA (0.02 M) for 6 h in water bath at 60˚C. The suspension was also

Table 1
The selected physicochemical properties of TBBPA

Abbreviation	Chemical structure	MW	Sw	pK_a	Density	MV	log K_{ow}
TBBPA		543.9	8.5	7.5–8.5	2.100	259	4.50

[a]MW: molecule weight (g/mol); Sw: aqueous solubility (umol/L); Density (g/cm^3); MV: molar volume (cm^3/mol); K_{ow}: octanol–water partition coefficient.

filtered by vacuum filtration and washed several times with distilled water. The resulted sample was dried at 65˚C. For reference, the material that resulted from modification will be known as TASSMt. Finally, TAMt and TASSMt were mechanically ground with a mortar and pestle to less than 200 mesh.

The transition metals-modified TAMt and TASSMt were prepared by mixing (2 g) of TAMt or TASSMt with a 0.1 M aqueous solution of corresponding M^{2+} nitrate (M=Co, Ni, or Cu) solution for 72 h in water bath at 60˚C. The suspension was then filtered by vacuum filtration and washed several times with distilled water and dried at 65˚C. These materials will be referred to as CoTAMt, NiTAMt, CuTAMt, CoTASSMt, NiTASSMt, and CuTASSMt, respectively.

2.3. Characterization methods

X-ray powder diffraction patterns were obtained using a Rigaku D/MAX2200 diffractometer operated at 30 kV and 30 mA with Cu K_α radiation. The XRD patterns were recorded from 4˚ to 60˚ of 2θ with a scan speed of 4˚/min. Fourier transform infrared (FTIR) spectra were recorded with a KBr pellet on a Thermo Nicolet-IS10 FTIR spectrometer in the spectral range of 4,000–400 cm^{-1}. Scanning electron microscopy (SEM) micrographs were obtained using a Gemini Leo 1550 instrument attached an X-ray energy dispersive spectrometer, EDS. Before scanning process, all samples were dried and coated with gold to enhance the electron conductivity. Nitrogen sorption–desorption experiments were carried out at 77 K on Micromeritics ASAP 2020 surface area and porosity analyzer (Quantachrome, United states). The samples were outgassed for 6 h at 200˚C before the sorption measurements. Specific surface area was calculated on the basis of the multi-point BET equation. Thermogravimetry analysis (TGA) is performed on a NETZSCH TG–DTA instrument at a heat rate of 5˚C/min from 25˚C to a maximum temperature of 800˚C under air atmosphere.

2.4. Batch experiments

TBBPA sorption were determined after mixing of 0.8 mg of IOMt and modified IOMt with 20 mL of TBBPA solution (0.2–2.0 mg L^{-1}) by shaking for certain time. Batch experiment was also conducted in triplicate. The tubes were centrifuged to separate solid and solution phase. Then, 2 mL of each solution was collected in clean vials for TBBPA analysis as above. Thermodynamic experiments were conducted at 288, 298, and 313 K.

The content of each sample was determined by high-performance liquid chromatography (HPLC) (Shimadzu LC-20AT, Kyoto, Japan) equipped with a photodiode array detector (SPD-M2OAV) and a VP-ODS column (150 × 4.6 mm, 5 μm) under the following condition: 80% methanol: 20% water with a wavelength of 209 nm for analysis of TBBPA. The injection volume was 20μL for all the solutions. The column was operated at 35˚C. All of the solution was injected at a flow of 0.8 mL min^{-1}.

The pH effect of TBBPA sorption on organic modified clays was investigated in a pH range from 3.0 to 11.0, using HCl or NaOH. The initial concentration of TBBPA solution was 1.0 mg L^{-1}. After shaking and centrifugation, the pH value of supernatants was detected by EL20 pH meter (Mettler Toledo Instruments Co., Ltd (Shanghai, China)).

3. Results and discussion

3.1. XRD and FTIR analysis

The XRD patterns of original and modified montmorillonite are shown in Fig. 1. The basal spacing of original montmorillonite was 1.52 nm. After pillared treatment by Al_{13}, it was increased to 1.71 nm, which was consistent with the values reported elsewhere [10]. The changes observed in the basal spacing were attributed to the expansion of montmorillonite interlayer by occupancy of Al_{13} species. The basal spacing of TMAB-Al_{13}-Montmorillonite (TAMt) was 1.72 nm, indicating that TMAB did not increase the interlayer distance of any further. For TMAB-SSTA-Al_{13}-montmorillonite (TASSMt), the basal space was 1.80 nm, corresponding to a bigger spacing distance. It suggested the added opposite charge surfactant resulted in the expansion of the interlayer space. When transition metals were incorporated onto the

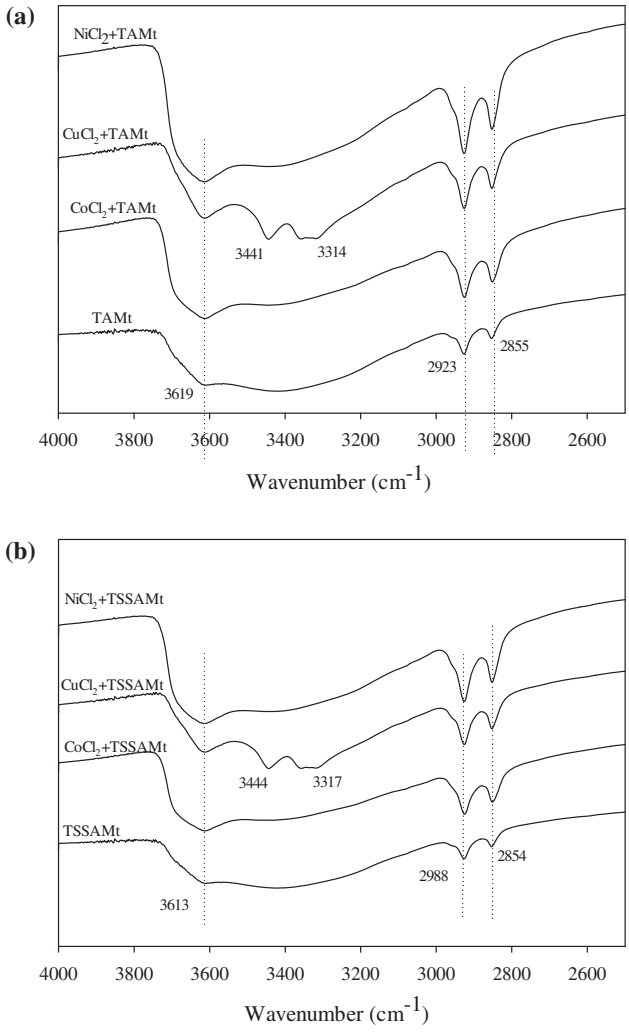

Fig. 1. FTIR for transition metals-modified organic–inorganic montmorillonite. (a) TMAB-Al_{13}-montmorillonite (TAMt) and transition metals-modified TMAB-Al_{13}-montmorillonite and (b) TMAB-SSTA-Al_{13}-montmorillonite (TSSAMt) and transition metals-modified TMAB-SSTA-Al_{13}-montmorillonite.

IOMt samples, XRD data for the resulting materials showed no further changes in basal spacing. However, the basal peak of IOMt became more symmetrical and intense after Cu^{2+} treatment. Meanwhile, new peaks appeared in XRD patterns of Cu^{2+}-modified IOMt. This phenomenon was attributed to a more order or higher crystallinity for modified IOMt, probably resulting from a change in the conformation and arrangement of the surfactants. Fig. 1 also shows the infrared spectra of IOMt in the absence and presence of transition metals. As shown in Fig. 1, the sorption bands at 3,619 cm^{-1} corresponded to the –OH stretching vibration. All the samples had the characteristic sorption bands of symmetric and asymmetric stretching vibration of the $–CH_2$ and $–CH_3$ at around 2,923–2847 cm^{-1} [20]. The bands between 3,314 and 3,347 cm^{-1} observed in Cu^{2+}-modified IOMt was possibly assigned to hydrogen bonding or cationic hydration.

3.2. TGA analysis

Fig. 2 gave the thermogravimetric (TGA) profile of IOMt in the absence and presence of transition metals. The TGA profile of original montmorillonite and Al_{13} pillared montmorillonite was also presented for comparison. As shown in Fig. 2, the mass loss of montmorillonite from 25 to 175˚C was 17%, corresponding to the dehydration of physically adsorbed water and water molecules around cation on exchangeable site in montmorillonite. The second mass loss was observed between 600 and 800˚C, which could be attributed to the dehydroxylation of montmorillonite structure [20]. Compared to montmorillonite, Al_{13}-pillared montmorillonite exhibited a less weight loss profile in the whole thermal treatment process, indicating adsorbed water in the surface was decreased with increasing Al_{13}. The presence of pillared inorganic materials could enhance thermal stability of montmorillonite.

For TAMt and TASSMt, four distinct steps were observed in Fig. 2. The first step was observed along the temperature range of 25–150˚C, associated with the loss of physically adsorbed water. The second steps were local at 150–70˚C and correspond to loss of –OH of Al_{13}, which resulted in converting Al_{13} to Al_2O_3. An obvious weight loss that occurred in the range of 270–400˚C could be attributed to the decomposition/evaporation of surfactants. The weight loss of original IOMt in the temperature range of 25–400˚C was much smaller than original montmorillonite, reflecting that the surfactants change the surface property of montmorillonite from hydrophilic to hydrophobic, and these data were a strong evidence of effective intercalation of surfactants in montmorillonite. The final step in the range of 400–800˚C was related to the dehydroxylation of montmorillonite structure. The weight loss in the temperature range of 270–400˚C for TASSMt was larger than that of TAMt, which implied that the anion surfactant SSTA was successfully intercalated into the interlayer of montmorillonite. Besides, the TGA profiles of transition metals-modified IOMt were similar to those of original IOMt, suggesting surfactants loading remain constant after modification of transition metals.

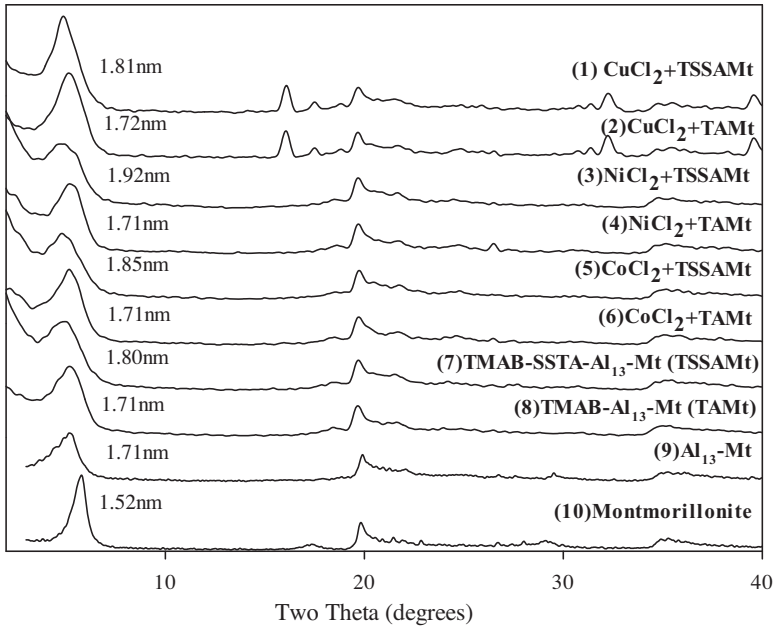

Fig. 2. XRD for transition metals-modified organic–inorganic montmorillonite. (1)–(2) Cu^{2+}-modified organic–inorganic montmorillonite; (3)–(4) Ni^{2+}-modified organic–inorganic montmorillonite; (5)–(6) Co^{2+}-modified organic–inorganic montmorillonite; (7) TMAB-SSTA-Al_{13}-montmorillonite; (8) TMAB-Al_{13}-montmorillonite; (9) Al_{13}-pillared montmorillonite; (10) montmorillonite.

3.3. SEM–EDS analysis

Scan electron microscopy for IOMt modified with transition metals is shown in Fig. 3. As reported in previous research, the aggregates of raw montmorillonite contained different particles with rough surface and outlines, resulting in an increase in specific surface area, especially for the external specific surface area [21]. After organic treatment, the surface roughness of organic–montmorillonite was decreased due to that the comb-like texture on the edge of particles of montmorillonite was replaced by surfactants with smooth boundary [22]. When the transition metals were introduced into the materials, the surface of IOMt did not undergo morphologic changes, indicating that strong interaction between montmorillonite and surfactants preserved the structure of layered clays. Compared with TASSMt, TAMt exhibited a more porous surface, suggesting that anion surfactants that were adsorbed on the surface of materials change, leading to a decrease in porosity. Meanwhile, it was noteworthy that some agglomeration of small particles (some white strip) was spread along at the edges of the clay layers and near the voids, especially for Cu^{2+}-modified materials. It seemed that the transition metals were more likely to be placed on the surface of IOMt and barely intercalated into the interlayer of adsorbents. Valentina Belova et al. [23] reported similar phenomenon about the Au particles adsorbed onto the edges of IOMt layers. They revealed that increasing the concentration of Au particles resulted in the more aggregation of Au particles on the surface of clays. In general, modification process did not affect the integrity of TMAB-Al_{13}-montmorillonite and TMAB-SSTA-Al_{13}-montmorillonite supports.

The results of chemical analysis of IOMt modified with transition metals were obtained using EDS data. The transition metals content normalized by silica present in sample ($\eta_{metals}/\eta_{silica}$, molar ratio) was 0.017, 0.026, and 0.242 for Co-, Ni-, and Cu-TAMt samples, respectively. Meanwhile, the transition metals content normalized by silica present in sample was 0.002, 0.016, and 0.182 for Co-, Ni-, and Cu-TASSMt samples, respectively. For both TAMt and TASSMt, the transition metals loading followed the order: Co < Ni < Cu. Difference in loadings could be attributed to ion exchange equilibrium limitations and transition metals hydrolysis phenomena. In addition, the transition metal content of TAMt was larger than that of TASSMt, suggesting that the presence of SSTA depressed the metal loading process.

3.4. Sorption and desorption isotherms of nitrogen

Fig. 4 showed the nitrogen sorption-desorption isotherms of TAMt and CuTAMt. As shown in Fig. 4,

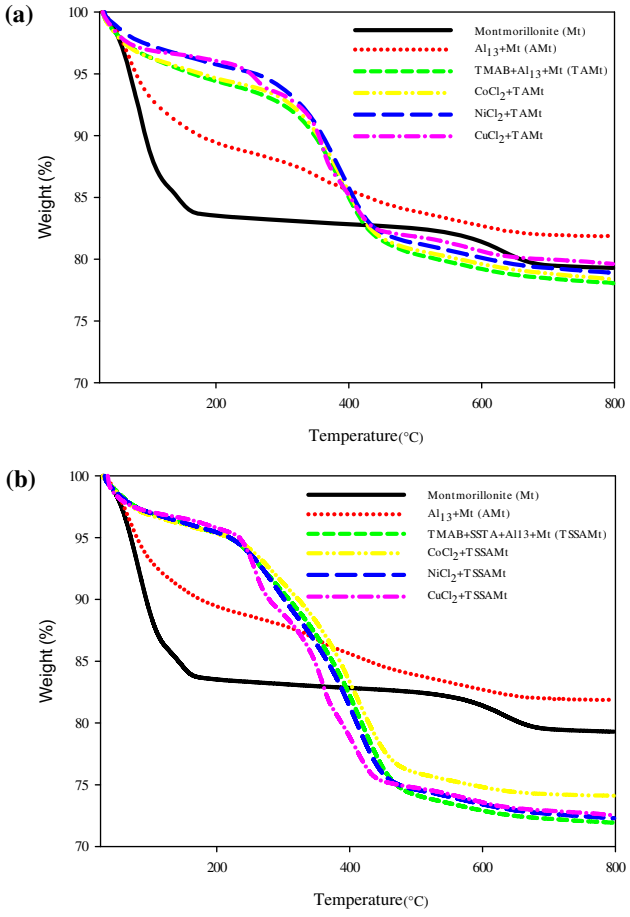

Fig. 3. TGA curves of raw and modified montmorillonite. (a) Raw montmorillonite and transition metals-modified TMAB-Al_{13}-montmorillonite (TAMt) and (b) raw montmorillonite and transition metals-modified TMAB-SSTA-Al_{13}-montmorillonite (TSSAMt).

TAMt and CuTAMt displayed type IV isotherms in the IUPAC classification [24]. The loops of TAMt and CuTAMt were conspicuous, sloping upward and parallel over a wide range of P/P_0, indicating that the hysteresis loops were likely to correspond to the type H_3 [21] The type H_3 loop should be considered as the type of montmorillonite, corresponding to aggregates of plate-like particles giving rise to slit-shaped pores [25]. The desorption branch of isotherms showed an inflection point "Knee" at about 0.45–0.50 P/P_0, which had been observed for many different types of layered materials when using nitrogen as the adsorptive. The result was attributed to complexity of capillary condensation in pore networks with pore blocking effects, namely "tensile strength artifact" [21].

The structural parameters of TAMt and CuTAMt, including Burne–Emmet–Teller (BET) surface area, micropore volume ($V_{micropore}$), and fractal dimension (D) values are summarized in Table 2. The specific surface area of TAMt and CuTAMt was 7.651 and 4.838 m^2/g, which was very small in comparison with SSA of untreated montmorillonite as reported elsewhere [10]. It was attributed to that the whole volume of interlayer space of montmorillonite was taken up by the alkyl chains and N_2 molecular could not enter. Despite the lower SSA, TAMt indeed contained small amounts of effective micropores arising from the surfactants addition [21]. In this work, $V_{micropore}$ of CuTAMt was smaller than that of TAMt. TGA profile had suggested that the existence of transition metals did not change the amounts of surfactants intercalated in the montmorillonite. The decreased SSA and $V_{micropore}$ [26] were possibly due to structural change of surfactants-modified montmorillonite resulted from the existence of Cu^{2+}. The fractal dimension (D) for modified montmorillonite was always related to the external surface characterization. Two methods including Frenkel–Halsey–Hill method and Neimark–Kiselev method were chosen to calculate the D values [27]. The fractal dimension (D) assumed value between 2 (smooth surface) and 3 (for rough surface). As shown in Table 2, D_N and D_F of TAMt were a little bigger than that of CuTAMt, which suggested that the Cu^{2+} might have a weak effect on the surface morphology of organic–montmorillonite.

3.5. TBBPA sorption isotherms

Equilibrium data were important for the design of sorption system. In this work, Langmuir, Freundlich, and Redlich–Peterson models were applied to describe the sorption equilibrium.

The Langmuir model assumed monolayer sorption onto a surface which consisted of finite number of active sites having a uniform energy, so the saturated monolayer isotherm can be represented as:

$$q_e = \frac{q_m K_L C_e}{1 + K_L C_e} \quad (1)$$

where C_e (mg/L) is the equilibrium concentration, q_e (mg/g) is the amount of TBBPA adsorbed onto per unit mass of adsorbent at equilibrium, q_m (mg/g) is the maximum sorption capacity which was correlated with monolayer coverage, and K_L (L/mg) is the Langmuir constant which was correlated with the affinity of the binding sites and sorption energy.

The Freundlich model can be expressed as:

$$q_e = K_f C_e^n \quad (2)$$

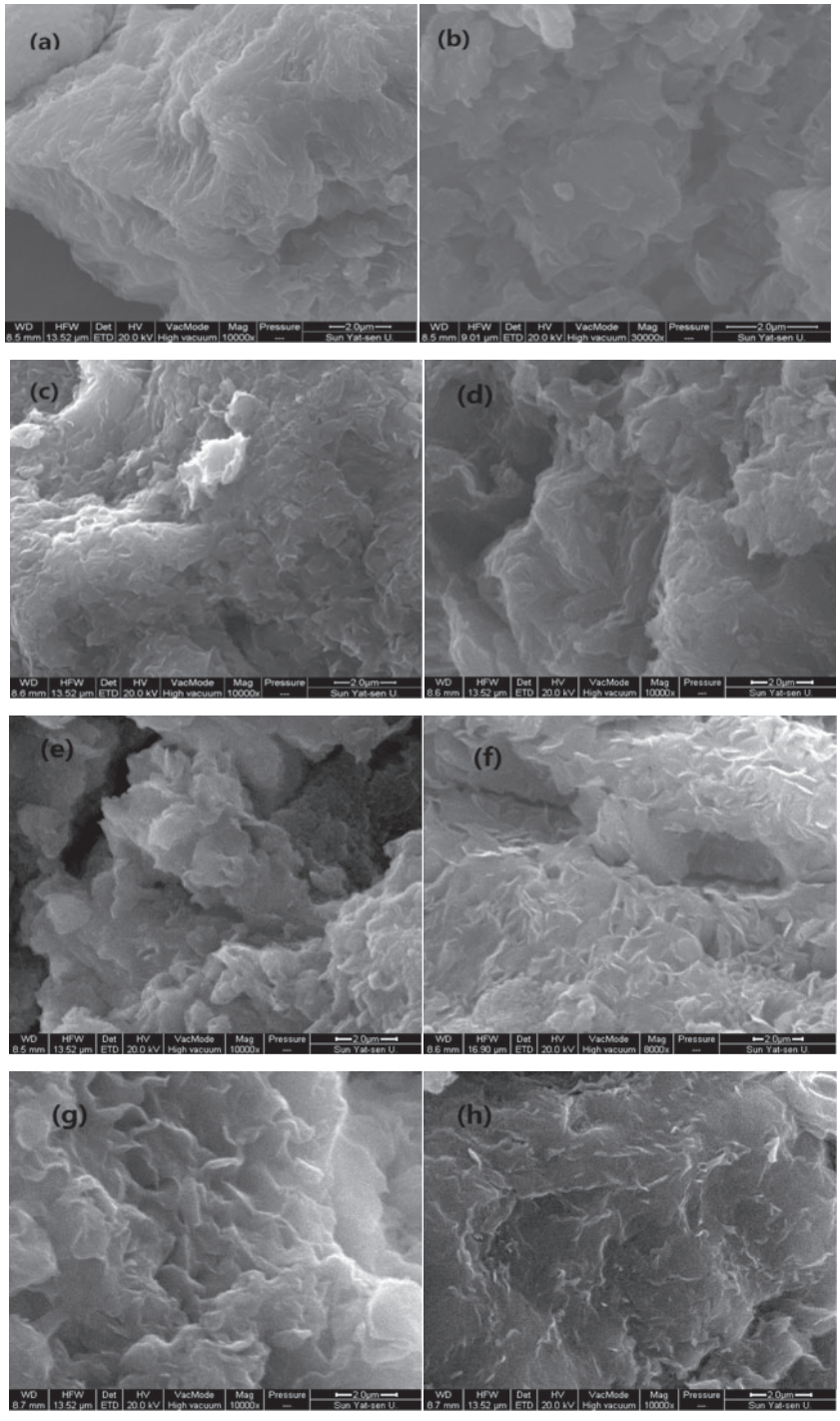

Fig. 4. Scanning electron microscopy micrographs for (a) ACMt, (b) ACSSMt, (c) CoACMt, (d) CoACSSMt, (e) NiACMt, (f) NiACSSMt, (g) CuACMt, and (h) CuACSSMt.

where K_f (L/g) was the Freundlich constant which was correlated with the capacity of sorption; n was an indicator of sorption intensity. The Freundlich model was employed to describe a heterogeneous system and reversible sorption and was not confined to the monolayer. The higher value of K_f indicated a higher affinity for sorption onto adsorbent and value of n ($0.1 < n < 1$), indicating that the sorption process is favorable.

Table 2
Specific surface area, micropore volume, and fractal dimension values of ACMt and CuACMt

Sample	SSA ($m^2 g^{-1}$)	S_{ext}[a] ($m^2 g^{-1}$)	S_{int} ($m^2 g^{-1}$)	$V_{micropore}$[b] ($ml g^{-1}$)		Fractal dimensions[c]	
				DR	BJH	NK	FHH
AlCMt	7.615	7.615	0.000	0.033	0.105	2.92	2.54
CuAlCMt	4.838	4.838	0.000	0.011	0.085	2.83	2.46

[a]Specific external surface areas (Sext) obtained from the *t*-method.
[b]Micropore volume calculated from the t curve with the method of De Boer et al. [26].
[c]Fractal dimension value calculated from Frenkel–Halsey–Hill (FHH) and Neimark–kiselev (NK) method [27].

The Redlich–Peterson model was given by equation as follows:

$$q_e = \frac{AC_e}{1 + BC_e^g} \tag{3}$$

where A (L/g), B (L/mg^g), and g are the Redlich–Peterson parameters, g is between 0 and 1. Redlich–Peterson equation was the compromise between Langmuir and Freundlich. For $g = 1$, Eq. (3) converts to the form of Langmuir model. The relevant parameters were obtained on the basis of the three parameter model at different temperatures. This isotherm combines both the characteristics of the Langmuir and Freundlich into a single equation.

The coefficient of determination (R^2) was calculated as follows:

$$R^2 = 1 - \frac{\sum_{i=1}^{n}(yi - \hat{y})^2}{\sum_{i=1}^{n}(yi - \bar{y})^2} \tag{4}$$

The relative parameters for isotherm and kinetic equation were calculated employing the variation χ^2 between the experimental data and calculated data using nonlinear regression analysis. The expression for χ^2 can be given as:

$$\chi^2 = \sum \frac{(q_{e,exp} - q_{e,calc})^2}{q_{e,calc}} \tag{5}$$

where $q_{e,calc}$ was the calculated sorption capacity of TBBPA adsorbed onto adsorbent which was correlated with the various sorption models; $q_{e,exp}$ was correlated with the experimental data of sorption capacity.

Fig. 5 shows the sorption isotherms of TBBPA on IOMt and transition metals-modified IOMt. As shown in Fig. 5, sorption capacity was increased with increasing equilibrium concentration of TBBPA. None of the isotherms data showcased an apparent adsorbent saturation. For TMAB-modified materials, CuTAMt exhibited the best interaction with TBBPA. NiTAMt also had better affinity for TBBPA than that of original TAMt. However, the existence of $CoCl_2$ did not significantly influence sorption of TBBPA on TAMt. Generally, equilibrium isotherm data for TMAB-modified materials presented that the affinity increased as follows: original ≈ Co < Ni < Cu. This trend was consistent with the order of the metal loading as shown in SEM-EDS data, suggesting that transition metal loading was a key factor for sorption of TBBPA on transition metals-modified IOMt. Similar result was also observed for TBBPA sorption on TMAB-SSTA-modified materials. Moreover, the increased sorption capacity brought by the transition metals suggested that TBBPA was plausibly forming complexes, these between the aromatic rings of TBBPA and transition metal centers, and based on an electron donation and back-donation process. Additionally, it was observed from the Fig. 5 that at low initial concentration of TBBPA, incorporation of transition metal did not tend to significantly increase the TBBPA sorption capacity of IOMt. However, at the other concentration end, the sorption isotherms indicated better affinity between the adsorbate and adsorbent modified with copper and nickel (seen Fig. 5). This was probably due to that the dominant mechanism at low concentration was only based on the hydrophobicity, while at high concentration, it was assigned to a combination of hydrophobicity and interaction with transition metals. This result indicated that high concentration was favorable for the formation of complexation between TBBPA and transition metals.

The TBBPA isotherms as shown in Fig. 5 were fitted curves by the Langmuir, Freundlich, and Redlich–Peterson models. The parameters of the three models calculated on the basis of Eqs. (1), (2), and (3) are listed in the Table 3. On the basis of R^2, χ^2, and the experimental results depicted in Table 3,

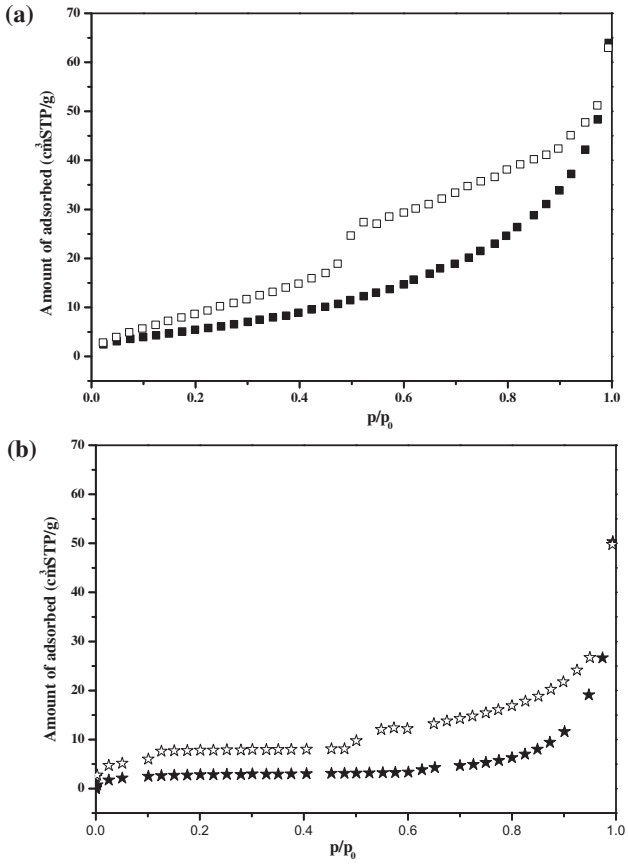

Fig. 5. Nitrogen adsorption–desorption isotherms (77 K) of (a) ACMt and (b) CuACMt (★ and ■-sorption; ☆ and □-desorption).

Freundlich model and Redlich–Peterson model fitted the experimental data well. However, most of the constant (g) of Redlich–Peterson isotherm was bigger than 1 or smaller than 0, which means that the isotherms were not suitable for Redlich–Peterson model. Thus, Freundlich model was chosen as the most suitable to describe the equilibrium experimental data. The n values of Freundlich model estimated from original IOMt were smaller than one, suggesting that the sorption was favorable and heterogeneous. The heterogeneity factors were expected since the IOMt contain both inorganic and organic moieties that could play individual or simultaneous roles as the sorption sties [11]. After incorporation of transition metals, the n value was increased to 1 or exceeded to 1, suggesting the homogeneous sorption sites were increased. This indicated that the transition metals were likely to influence the arrangement of sorption sites. The sorption affinity coefficient (K_f) of TAMt was lower than that of TASSMt due to higher hydrophobicity resulted from the addition of SSTA. However, after the transition metals loading, CuTAMt showcased a better sorption capacity for TBBPA than CuTASSMt as evident by isotherms in Fig. 5 and fitting data in Table 3, which possibly resulted from a higher metal loading for CuTAMt. This result suggested that the main sorption mechanism was complex interaction between TBBPA and Cu^{2+} rather than hydrophobicity.

3.6. Sorption kinetics

Three kinetic models including pseudo-first-order model, pseudo-second-order model, and intraparticle diffusion model were used to examine the controlling mechanism of the sorption process and also to test the experimental data. The equations are given as follows [28]:

$$\ln(q_e - q_t) = \ln q_e - k_1 t \tag{6}$$

$$\frac{t}{q_t} = \frac{1}{(k_2 q_e^2)} + \frac{1}{q_e} t \tag{7}$$

$$q_t = k_i t^{0.5} + c \tag{8}$$

where q_e and q_t are the amounts of TBBPA adsorbed (mg/g) at equilibrium and time t (min), respectively; k_1 and k_2 are the rate constant of first-order and second-order sorption (min^{-1}); the parameters could be determined from the linear plots of $\ln(q_e - q_t)$ vs. t and t/q_t vs. t, respectively (Fig. 6(b)–(c)); k_i is the rate constant of intraparticle diffusion (mg/g $min^{0.5}$) and is determined from the linear plots of q_t vs. $t^{0.5}$ (Fig. 6(d)). The value of c related to the thickness of the boundary layer.

Kinetic data obtained from above models are listed in Table 4, which shows that coefficient of determination (R^2) values for the pseudo-second-order kinetic model were over 0.99 for both CuTAMt and CuTASSMt. The experimental q_e values agree well with the calculated values obtained from the pseudo-second-order. The χ^2 obtained from pseudo-second-order model was smaller than that of pseudo-first-order model. The results indicated that pseudo-second-order model appeared to the better model for sorption of TBBPA onto Cu^{2+}-modified IOMt. Based on this model, a chemisorption reaction could be predominant in the rate-controlling step [29]. The second-order rate constants were used to calculate the initial sorption rate given by $H = k_2 q_e^2$ shown in Table 4. It was found that the initial sorption rate of CuTASSMt was larger than that of CuTAMt. This effect was attributed to more available hydrophobic phase which was created

Table 3
Models fitting parameters for TBBPA adsorption isotherms on IOMt and transition metals-modified IOMt[a]

	TAMt				TASSMt			
	None[b]	Co^{2+}	Ni^{2+}	Cu^{2+}	None[b]	Co^{2+}	Ni^{2+}	Cu^{2+}
	Freundlich							
K_f	33.32 ± 4.10	37.68 ± 4.30	52.57 ± 5.04	417.64 ± 167.82	34.28 ± 1.85	21.51 ± 2.14	48.78 ± 6.71	120.75 ± 28.52
n	0.58 ± 0.13	0.85 ± 0.15	0.82 ± 0.10	1.76 ± 0.27	0.70 ± 0.06	0.77 ± 0.16	1.09 ± 0.18	1.63 ± 0.25
R^2	0.93	0.95	0.98	0.96	0.98	0.92	0.95	0.96
χ^2	5.84	4.00	2.77	5.64	2.78	1.61	5.30	6.29
	Langmuir							
q_m	46.24 ± 11.85	76.99 ± 95.06	107.29 ± 60.64	765.33 ± 158.97	60.12 ± 9.76	53.77 ± 33.33	366.17 ± 192.52	1,414.16 ± 365.17
K_L	2.06 ± 1.01	0.73 ± 1.19	0.75 ± 0.56	0.16 ± 3.61	1.14 ± 0.29	0.63 ± 0.56	0.13 ± 0.72	0.04 ± 1.13
R^2	0.89	0.84	0.97	0.71	0.97	0.86	0.84	0.82
χ^2	4.49	4.18	3.14	14.98	0.80	4.76	5.14	51.27
	Redlich–Peterson							
A	70.97 ± 16.50	59.07 ± 12.89	158.94 ± 47.45	175.57 ± 54.05	59.24 ± 13.13	35.61 ± 9.47	369.26 ± 94.17	238.41 ± 47.32
B	1.63 ± 0.61	0.61 ± 3.11	2.08 ± 2.48	0.002 ± 0.01	0.85 ± 0.34	0.71 ± 2.26	6.24 ± 4.53	1.53 ± 3.02
G	2.08 ± 1.47	0.59 ± 3.31	0.31 ± 1.80	−3.17 ± 2.70	1.34 ± 0.95	0.94 ± 3.47	−0.02 ± 1.36	−0.06 ± 3.33
R^2	0.91	0.91	0.97	0.93	0.98	0.86	0.89	0.88
χ^2	3.94	3.96	2.81	32.88	0.79	4.75	5.93	29.26

[a]K_f (L/g), q_m (mg/g), K_L (L/mg), A (L/g), B (L/mg^g).
[b]None = adsorbents without transition metals.

by SSTA. It also demonstrated that the sorption process firstly occurred on the surface of organic surfactants, and then followed by the interaction between TBBPA and transition metals. On the whole, this process of sorption of TBBPA on Cu^{2+}-modified IOMt was very quick in the beginning and equilibrium time was very short.

The intraparticle diffusion model was also investigated to figure out the sorption mechanism. Fig. 6(d) shows that the plots of q_t against $t^{0.5}$ consist of two separate linear regions. Such multiple linear plots indicated two sorption steps occurred. The first step could be attributed to the instantaneous sorption or external surface sorption, the second to intraparticle diffusion [30,31]. As seen from Table 4, the c value was larger than zero, which indicated that the intraparticle diffusion was not the only rate-limiting mechanism in the sorption process. Some other mechanism such as complexation along with intraparticle diffusion was also involved.

3.7. Thermodynamics

The thermodynamic parameters, such as free energy (ΔG), enthalpy change (ΔH), and entropy change (ΔS), were calculated at temperature of 288, 298, and 313 K to find the feasibility and exothermic based on the methods according to Fasfous Ismail I. et al. [18].

The constant K_0 can be defined as:

$$K_0 = \frac{\alpha_q}{\alpha_c} = \frac{\gamma q_e}{\gamma C_e} = \frac{q_e}{C_e} \tag{9}$$

where α_q is the activity of adsorbed TBBPA, and α_c is the activity of TBBPA in solution at equilibrium, and γq_e and γC_e are the activity coefficient. Since the concentration of TBBPA in solution approaches zero, the activity coefficient approached unity. The value of K_0 was confirmed through plotting the $\ln K_0$ vs. q_e, and exploring the q_e to zero. The straight line obtained was fitted using linear least squares analysis methods. The intercept of vertical axis was regarded as $\ln K_0$.

The free energy (ΔG), enthalpy change (ΔH), and entropy change (ΔS) were calculated by the equation as follows:

$$\Delta G = -RT \ln K_0 \tag{10}$$

$$\ln K_0 = -\frac{\Delta H}{RT} + \frac{\Delta S}{RT} \tag{11}$$

where R is universal gas constant (8.314 J/mol K), and T is the sorption temperature in Kelvin. The value of ΔH is confirmed by the slope of Eq. (11). All of the results are presented in Table 5. The negative values of ΔG and positive values of ΔH corresponded to that the sorptions of TBBPA onto CuTAMt and CuTASSMt were spontaneous and endothermic. The values of ΔG decreased with the increase in temperature, indicating the endothermic sorption of TBBPA onto CuTAMt and CuTASSMt was enhanced by an increase in temperature. The values of ΔH were high enough to ensure strong interaction between TBBPA and Cu^{2+}-modified IOMt. The positive value of ΔS corresponds to an increase in degree of freedom of the adsorbed species. It was likely that TBBPA molecules on those adsorbents were more chaotically arranged compared to the situation in aqueous solution. The increased sorption capacity of CuTAMt and CuTASSMt at higher temperature was caused by the complexation between TBBPA and transition metals.

3.8. Effects of pH

TBBPA is an ionizable organic pollutant, so the sorption capacity may vary with pH. Fig. 7 shows the sorption capacity of TBBPA adsorbed by CuTAMt and CuTASSMt at different pH condition. The results showed that removal efficiencies of phenol were kept unchanged in the pH range of 3–6, but strongly decreased by about 86–91% when pH changed from 6 to 8. The apparent decrease at the higher pH is likely due to partial ionization of TBBPA. As shown in Table 1, the pK_a of TBBPA was 7.5 and 8.5. TBBPA mainly existed in anion forms ($TBBPA^-$ and $TBBPA^{2-}$) when the pH was above 8.5. The effect of repellency between the ionized TBBPA and the negative particles was enhanced at high pH region. Meanwhile, at alkaline pH condition, transition metals probably moved to the negatively charged silanol group, resulting in sites inaccessible to the TBBPA [10]. When the solution reached alkaline condition, little or no sorption of TBBPA indicated a potential adsorbent regeneration schemes.

3.9. Sorption mechanism

There were several possible mechanisms for the sorption of TBBPA, mainly including hydrophobic interaction, electrostatic interaction, complex formation, and hydrogen bonding. The sorption of TBBPA on original IOMt was mainly dominated by the hydrophobic interaction. The loaded surfactants

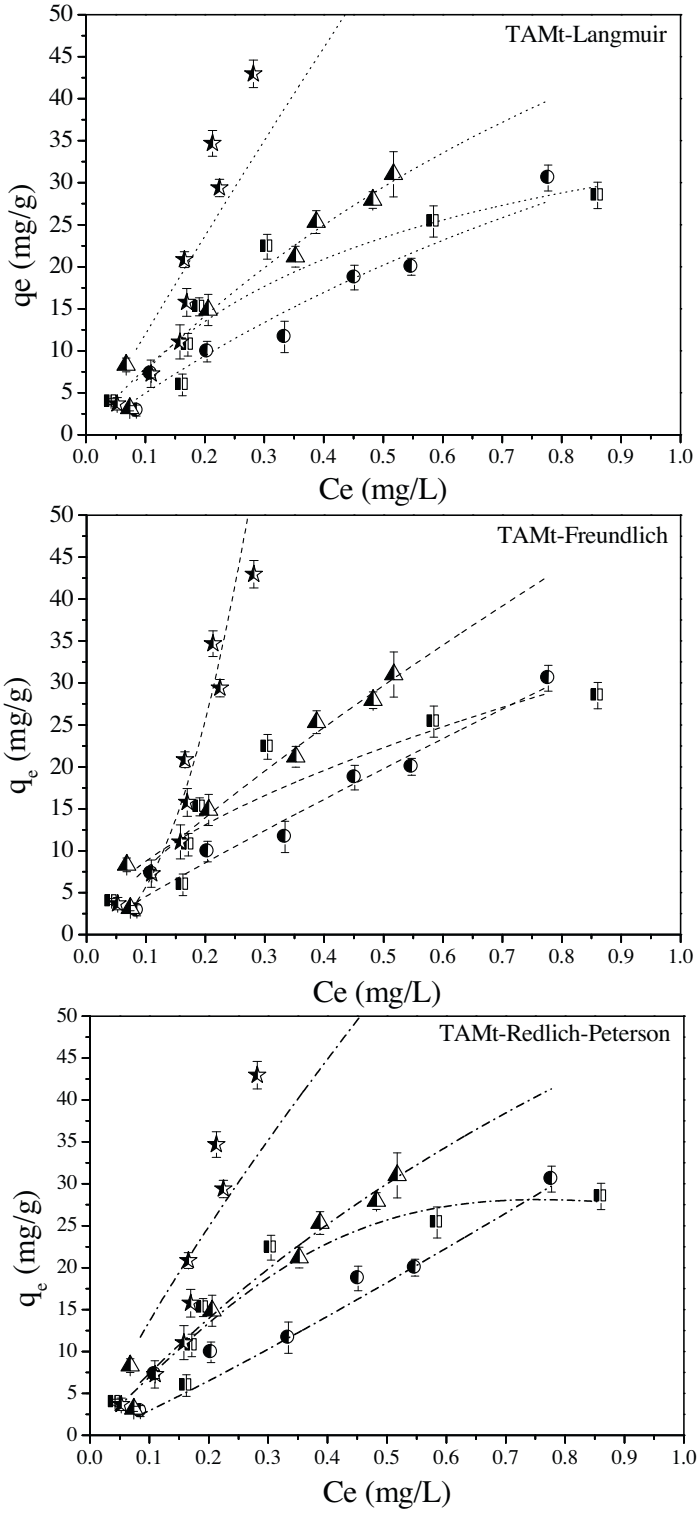

Fig. 6. Adsorption isotherms of TBBPA on TMAB-Al_{13}-montmorillonite (TAMt) and transition metals-modified TAMt, using a nonlinear regressive method (Adsorbents: 40 mg L^{-1}; contact time: 48 h; 298 K); — Freundlich fitted curves; .... Langmuir fitted curves; –.–. Redlich–Peterson fitted curves; ◧ TAMt, ◐ $CoCl_2$ + TAMt, ◭ $NiCl_2$ + TAMt, ✯ $CuCl_2$ + TAMt.

Table 4
Kinetic models parameters obtained from TBBPA adsorption on CuACMt and CuACSSMt[a]

Models		CuAlCMt	CuAlCSSMt
Pseudo-first-order model	$q_{e,exp}$	22.08 ± 2.45	21.35 ± 1.87
	k_1 (10^{-3})	7.01 ± 1.16	11.34 ± 1.42
	$q_{e,cal}$	6.65 ± 1.08	10.74 ± 2.19
	R^2	0.80	0.84
	χ^2	1.448	3.872
Pseudo-second-order model	k_2 (10^{-3})	3.67 ± 2.10	4.80 ± 3.24
	$q_{e,cal}$	22.23 ± 0.53	22.72 ± 0.61
	H	2.47 ± 1.89	2.48 ± 1.74
	R^2	0.99	0.99
	χ^2	0.395	2.441
Intraparticle diffusion model	k_i	0.42 ± 0.05	0.81 ± 0.10
	c	15.4 ± 0.57	8.98 ± 1.03
	R^2	0.86	0.85
	χ^2	0.423	2.545

[a]q_e (mg/g), k_1 (min^{-1}), k_2 (g/(mg min)), H (mg/(g min)) k_i (mg/g $min^{0.5}$), C (mg/g).

created the organic solvent-like hydrophobic phase and resulted in a strong attraction of TBBPA molecule with the IOMt through van der Waals interaction. Clays modified with alkylammonium ions absorbed hydrocarbons through partitioning to give linear sorption isotherms, whereas sorption of organic molecules having polar groups exemplified by phenolic compounds provided nonlinear isotherms due to the contribution of specific sorption [32]. The nonlinear Freundlich isotherms for TBBPA adsorbed by IOMt suggested that specific sorption rather than partition contributed to the main sorption mechanism. In addition, electrostatic interaction might be another explanation for TBBPA sorption. Yuri Park and coworkers [33] investigated the BPA sorption on organo-montmorillonite and identified that the loaded organic surfactants tended to develop more positive charge on the clay surfaces by shielding the negative charge, which led to greater attraction of the anionic forms of BPA. The dissociated BPA anions tended to associate with the positively charged head of surfactants on both inner and outer layers of the clays via electrostatic interaction [33]. Since TBBPA had a similar chemical structure to BPA and partly existed as anion molecule in neutral condition, it was probable that similar electrostatic interaction between IOMt and TBBPA on both inner and outer layers of clays was formed.

For both cationic and anionic–cationic surfactant-modified IOMt, the limited sorption of TBBPA was greatly enhanced by the incorporation of transition metals. A possible explanation suggested in this sorption system was the interaction brought by the presence of metals and TBBPA. As shown in Table 1, TBBPA has two aromatic rings and O–H groups which could form π-complexes with transition metals. The groups of TBBPA provided π-electrons for donation. The positive charge of transition metal was an electron

Table 5
The thermodynamics parameters for the sorption of TBBPA on Cu^{2+}-modified materials

Absorbent	Temperature (K)	ΔG (kJ/mol)	ΔH (kJ/mol)	ΔS (kJ/K mol)
CuAlCMt	288	−7.65	31.17	0.134
	298	−8.54		
	313	−11.02		
CuAlCSSMt	288	−5.21	27.39	0.113
	298	−6.56		
	313	−8.04		

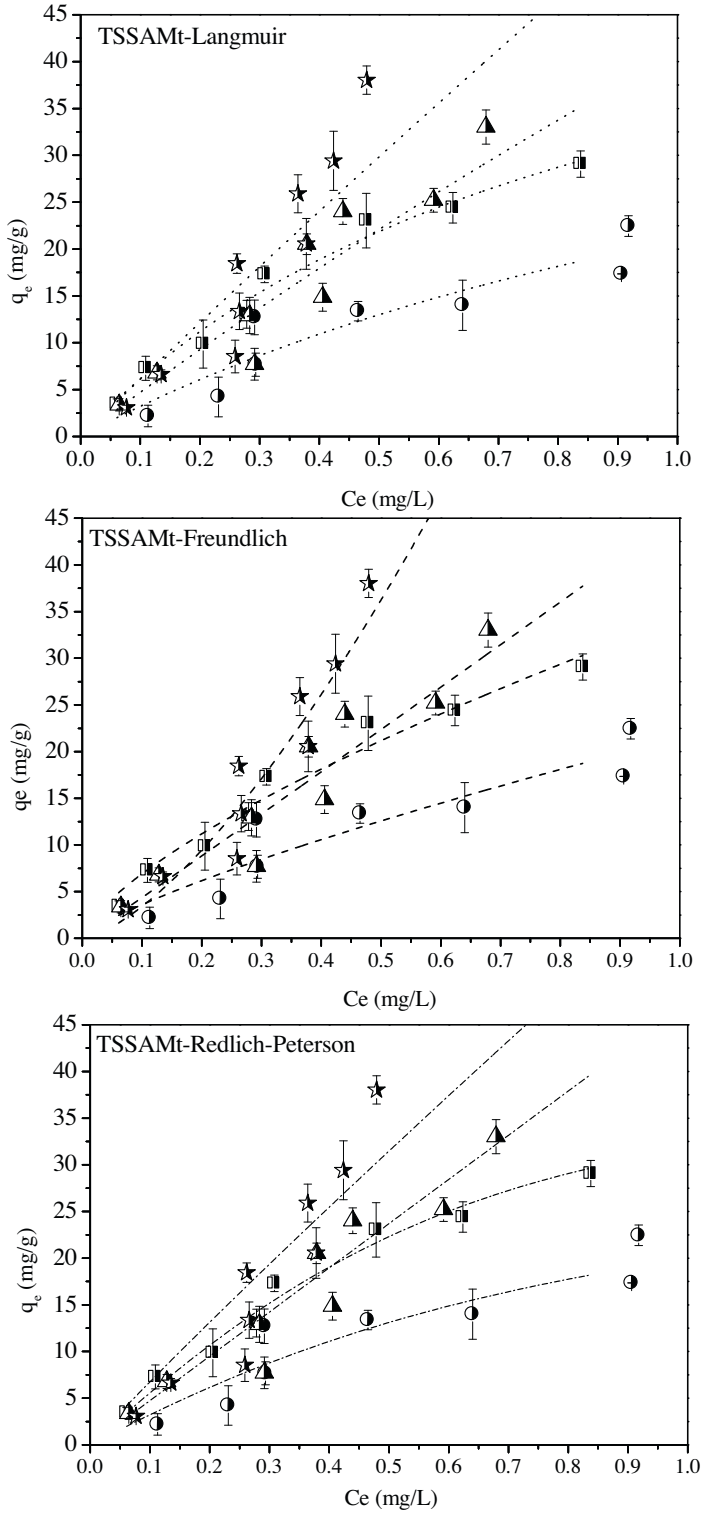

Fig. 7. Adsorption isotherms of TBBPA on TMAB-SSTA-Al_{13}-montmorillonite (TSSAMt) and transition metals-modified TSSAMt, using a nonlinear regressive method (Adsorbents: 40 mg L^{-1}; contact time: 48 h; 298 K); — Freundlich fitted curves; .... Langmuir fitted curves; –.–. Redlich–Peterson fitted curves; ◨ TSSAMt, ◑ $CoCl_2$+TSSACMt, ◭ $NiCl_2$+TSSAMt, ✯ $CuCl_2$+TSSAMt.

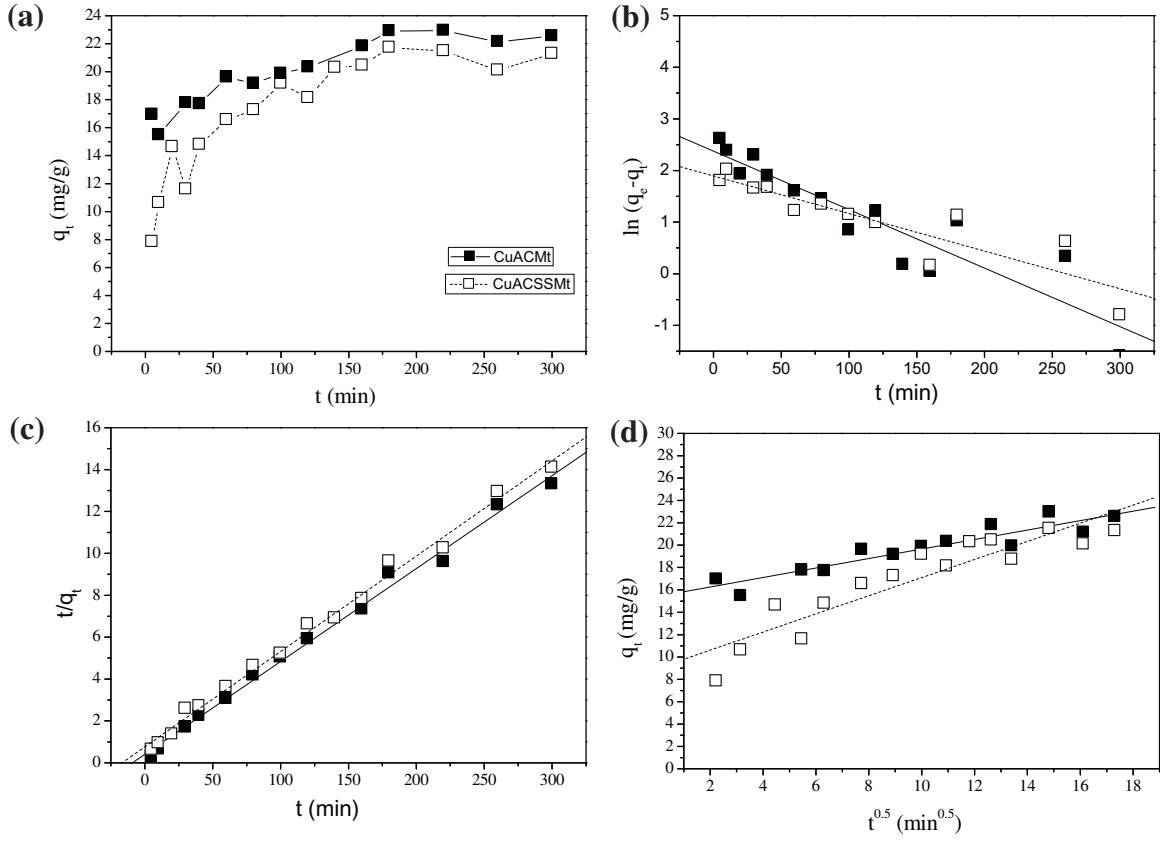

Fig. 8. (a) Effect of contact time on the uptake of TBBPA on CuTAMt (■) and CuTSSAMt (□); (b) plots of pseudo-first-order model; (c) plots of pseudo-second-order model; and (d) intraparticle diffusion model (initial concentration was 1.0 mg L^{-1}; adsorbent was 40 mg L^{-1};temperature was 298 K).

acceptor. In addition, it had been also reported that the copper-based variant could form water-bridging-type complexation with polar compounds in clays [34]. The water-bridging-type complexation between copper and TBBPA was possibly assigned to another complexation mechanism. Hydrogen bonding between the phenols groups and Si–O on montmorillonite should not be the dominant mechanism due to less sorption occurred in the untreated montmorillonite [32]. In general, TBBPA sorption on transition metals-modified IOMt was mainly attributed to hydrophobic interaction, electrostatic interaction, and complexation.

3.10. Comparison of the results with those obtained by other methods

It was evident from the results that Cu^{2+}-modified IOMt gave the best sorption capacity for TBBPA uptake. Although the obtained results cannot be directly compared with those obtained by the use of other adsorbents such as graphene oxide, MWCNTs, and fly ash, it appeared that the sorption by transition metals-modified IOMt was an effective method for the removal of TBBPA from aqueous solution. Yun Zhang [35] in the previous study compared the sorption capacity of different adsorbents for removing TBBPA from aqueous solution and concluded that the graphene oxide offered sorption capacity of 115.77 mg/g, which was the maximum sorption values obtained from the Langmuir model among six different adsorbents. In this work, the maximum sorption capacity obtained from the Langmuir model was 765.33 mg/g for CuTAMt and 1,414.16 mg/g for CuTASSMt. However, the Langmuir was not the best fitting model for TBBPA sorption in this study. Therefore, the sorption coefficient (K_f) obtained from Freundlich model at 298 K was chosen as another parameter for comparison. The values were 417.64 L/g for CuTAMt and 120.75 L/g for CuTASSMt, compared with 123.94 L/g by graphene oxide reported in the previous study [16]. It revealed that the Cu^{2+}-modified IOMt showed similar sorption capacity as graphene oxide. Given the relatively low cost of pro-

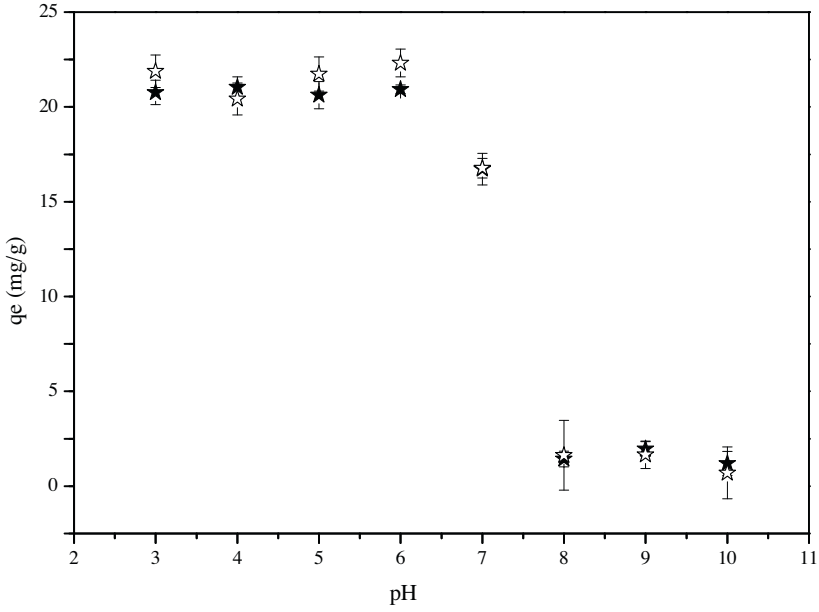

Fig. 9. Effect of pH on TBBPA adsorption by CuTAMt and CuTSSAMt (Adsorbent: 40 mg L^{-1}; contact time 48 h; 298 K); ★-CuTAMt; ☆-CuTSSAMt.

duction of transition metals-modified IOMt, they may offer significant advantages in the removal of industrial pollutants from the environment.

4. Conclusions

Transition metals (Cu^{2+}, Co^{2+}, and Ni^{2+})-modified different type of IOMts were synthesized and characterized by XRD, FTIR, TGA, SEM-EDS, and N_2 sorption–desorption isotherms analysis. Combination of XRD and FTIR showed that the existence of Cu^{2+} possibly influenced the structural characteristics of IOMt in spite of the type of surfactants components. The result of TGA indicated that transition metals did not influence the amounts of surfactants intercalated in the interlayer of montmorillonite. SEM exhibited that when the transition metals were introduced into the materials, non-obvious change of structure for those materials was observed in spite of organic component. Transition metals were probably aggregated on the edges of IOMt layers. Transition metals loading followed the order of Cu > Ni > Co. The specific surface area and micropore volume of CuTAMt obtained from Dubinin–Radushkevich (DR) and Barrett–Joyner–Halenda (BJH) model were smaller than that of TAMt. Freundlich model gave the best fit for sorption isotherms of TBBPA, and the acidic condition was favorable for TBBPA sorption. The removal efficiencies of TBBPA were kept unchanged in the pH range of 3–6, but strongly decreased by about 86–91% when pH changed from 6 to 8. Additionally, the Cu^{2+}-modified IOMt showed a same sorption capacity order as graphene oxide and much more low cost of production. Several mechanism involving hydrophobic interaction, electrostatic interaction, and donor–acceptor complexation with transition metals was provided to explain the sorption phenomenon.

Acknowledgment

This work was supported in part by the Grant from the Environmental and Pollution Control Technology and National Key Scientific and Technological Project ''Water Pollution Control and Treatment'' (2012ZX07206002) (2012ZX07206004).

References

[1] H. Zaghouane-Boudiaf, M. Boutahala, Adsorption of 2,4,5-trichlorophenol by organo-montmorillonites from aqueous solutions: Kinetics and equilibrium studies, Chem. Eng. J. 170(1) (2011) 120–126.
[2] O. Bouras, M. Houari, H. Khalaf, Adsorption of some phenolic derivatives by surfactant treated al-pillared Algerian bentonite, Toxicol. Environ. Chem. 70(1–2) (1999) 221–227.
[3] O. Bouras, M. Houari, H. Khalaf, Using of surfactant modified fe-pillared bentonite for the removal of pentachlorophenol from aqueous stream, Environ. Technol. 22(1) (2001) 69–74.
[4] O. Bouras, J.C. Bollinger, M. Baudu, H. Khalaf, Adsorption of diuron and its degradation products

from aqueous solution by surfactant-modified pillared clays, Appl. Clay Sci. 37(3–4) (2007) 240–250.
[5] H. Khalaf, O. Bouras, V. Perrichon, Synthesis and characterization of Al-pillared and cationic surfactant modified Al-pillared Algerian bentonite, Microporous Mater. 8(3–4) (1997) 141–150.
[6] P.X. Wu, Z.W. Liao, H.F. Zhang, J.G. Guo, Adsorption of phenol on inorganic–organic pillared montmorillonite in polluted water, Environ. Int. 26(5–6) (2001) 401–407.
[7] Z. Bouberka, A. Khenifi, H. Ait Mahamed, B. Haddou, N. Belkaid, N. Bettahar, Z. Derriche, Adsorption of Supranol Yellow 4 GL from aqueous solution by surfactant-treated aluminum/chromium-intercalated bentonite, J. Hazard. Mater. 162(1) (2009) 378–385.
[8] L. Yan, X. Shan, B. Wen, S. Zhang, Effect of lead on the sorption of phenol onto montmorillonites and organo-montmorillonites, J. Colloid Interface Sci. 308 (1) (2007) 11–19.
[9] N. Liu, M. Wang, M. Liu, F. Liu, L. Weng, L.K. Koopal, W.-f. Tan, Sorption of tetracycline on organo-montmorillonites, J. Hazard. Mater. 225–226 (2012) 28–35.
[10] W.A. Cabrera-Lafaurie, F.R. Román, A.J. Hernández-Maldonado, Transition metal modified and partially calcined inorganic–organic pillared clays for the adsorption of salicylic acid, clofibric acid, carbamazepine, and caffeine from water, J. Colloid Interface Sci. 386(1) (2012) 381–391.
[11] W.A. Cabrera-Lafaurie, F.R. Román, J. Arturo Hernández-Maldonado, Single and multi-component adsorption of salicylic acid, clofibric acid, carbamazepine and caffeine from water onto transition metal modified and partially calcined inorganic-organic pillared clay fixed beds. J. Hazard. Mater. 282 (2015) 174–182.
[12] Z. Hasan, J. Jeon, S.H. Jhung, Adsorptive removal of naproxen and clofibric acid from water using metal-organic frameworks, J. Hazard. Mater. 209–210 (2012) 151–157.
[13] I. Watanabe, T. Kashimoto, R. Tatsukawa, Identification of the flame retardant tetrabromobisphenol-a in the river sediment and the mussel collected in Osaka, Bull. Environ. Contam. Toxicol. 31(1) (1983) 48–52.
[14] U. Sellström, B. Jansson, Analysis of tetrabromobisphenol A in a product and environmental samples, Chemosphere 31(4) (1995) 3085–3092.
[15] J.W. Voordeckers, D.E. Fennell, K. Jones, M.H. Häggblom, Anaerobic biotransformation of tetrabromobisphenol A, tetrachlorobisphenol A, and bisphenol A in estuarine sediments, Environ. Sci. Technol. 36(4) (2002) 696–701.
[16] Y. Zhang, Y. Tang, S. Li, S. Yu, Sorption and removal of tetrabromobisphenol A from solution by graphene oxide, Chem. Eng. J. 222 (2013) 94–100.
[17] Z. Sun, Y. Yu, L. Mao, Z. Feng, H. Yu, Sorption behavior of tetrabromobisphenol A in two soils with different characteristics, J. Hazard. Mater. 160(2–3) (2008) 456–461.
[18] I.I. Fasfous, E.S. Radwan, J.N. Dawoud, Kinetics, equilibrium and thermodynamics of the sorption of tetrabromobisphenol A on multiwalled carbon nanotubes, Appl. Clay Sci. 256(23) (2010) 7246–7252.
[19] L. Zhu, R. Zhu, Simultaneous sorption of organic compounds and phosphate to inorganic–organic bentonites from water, Sep. Purif. Technol. 54(1) (2007) 71–76.
[20] D. Chen, J. Chen, X. Luan, H. Ji, Z. Xia, Characterization of anion–cationic surfactants modified montmorillonite and its application for the removal of methyl orange, Chem. Eng. J. 171(3) (2011) 1150–1158.
[21] J. Zhu, L. Zhu, R. Zhu, S. Tian, J. Li, Surface microtopography of surfactant modified montmorillonite, Appl. Clay Sci. 45(1–2) (2009) 70–75.
[22] S.M. Rivera-Jimenez, M.M. Lehner, W.A. Cabrera-Lafaurie, A.J. Hernández-Maldonado, Removal of naproxen, salicylic acid, clofibric acid, and carbamazepine by water phase sorption onto inorganic–organic-intercalated bentonites modified with transition metal cations, Environ. Eng. Sci. 28(3) (2011) 171–182.
[23] V. Belova, H. Möhwald, D.G. Shchukin, Ultrasonic intercalation of gold nanoparticles into a clay matrix in the presence of surface-active materials. part II: Negative sodium dodecylsulfate and positive cetyltrimethylammonium bromide, J. Phys. Chem. C 113(16) (2009) 6751–6760.
[24] W.A. Steele Adsorption surface area and porosity second ed., in: S.J. Gregg K.S.W. Sing, Academic Press, New York, NY, 1982, 312, $44.50, J. Colloid. Interf. Sci. 94 1983 597–598.
[25] Y. Gao, W. Li, H. Sun, Z. Zheng, X. Cui, H. Wang, F. Meng, A facile *in situ* pillaring method—The synthesis of Al-pillared montmorillonite, Appl. Clay Sci. 88–89 (2014) 228–232.
[26] J.H. De Boer, B.G. Linsen, ThJ Osinga, Studies on pore systems in catalysts: VI. The universal t curve, J. Catal. 4(6) (1965) 643–648.
[27] M.J. Watt-Smith, K.J. Edler, S.P. Rigby, An experimental study of gas adsorption on fractal surfaces, Langmuir 21(6) (2005) 2281–2292.
[28] Y. Shu, L. Li, Q. Zhang, H. Wu, Equilibrium, kinetics and thermodynamic studies for sorption of chlorobenzenes on CTMAB modified bentonite and kaolinite, J. Hazard. Mater. 173(1–3) (2010) 47–53.
[29] Y.S. Ho, G. McKay, The kinetics of sorption of divalent metal ions onto sphagnum moss peat, Water Res. 34(3) (2000) 735–742.
[30] R.S. Juang, F.C. Wu, R.L. Tseng, Mechanism of adsorption of dyes and phenols from water using activated carbons prepared from plum kernels, J. Colloid Interface Sci. 227(2) (2000) 437–444.
[31] G.M. Walker, L. Hansen, J.A. Hanna, S.J. Allen, Kinetics of a reactive dye adsorption onto dolomitic sorbents, Water Res. 37(9) (2003) 2081–2089.
[32] Q. Wei, T. Nakato, Competitive adsorption of phenols on organically modified layered hexaniobate K4Nb6O17, Microporous Mesoporous Mater. 96(1–3) (2006) 84–92.
[33] Y. Park, Z. Sun, G.A. Ayoko, R.L. Frost, Bisphenol A sorption by organo-montmorillonite: Implications for the removal of organic contaminants from water, Chemosphere 107 (2014) 249–256.
[34] M. Kowalska, H. Güler, D.L. Cocke, Interactions of clay minerals with organic pollutants, Sci. Total Environ. 141(1–3) (1994) 223–240.
[35] Y. Zhang, L. Jing, X. He, Y. Li, X. Ma, Sorption enhancement of TBBPA from water by fly ash-supported nanostructured γ-MnO2. J. Ind. Eng Chem 21(1) (2014) 610–619.